



Title	Production cross sections of deuteron-induced reactions on natural palladium for Ag isotopes
Author(s)	Ukon, Naoyuki; Aikawa, Masayuki; Komori, Yukiko; Haba, Hiromitsu
Citation	Nuclear Instruments and Methods in Physics Research Section B: Beam Interactions with Materials and Atoms, 426, 13-17 <a href="https://doi.org/10.1016/j.nimb.2018.04.019">https://doi.org/10.1016/j.nimb.2018.04.019</a>
Issue Date	2018-07-01
Doc URL	<a href="http://hdl.handle.net/2115/78743">http://hdl.handle.net/2115/78743</a>
Rights	© 2018. This manuscript version is made available under the CC-BY-NC-ND 4.0 license <a href="http://creativecommons.org/licenses/by-nc-nd/4.0/">http://creativecommons.org/licenses/by-nc-nd/4.0/</a>
Rights(URL)	<a href="http://creativecommons.org/licenses/by-nc-nd/4.0/">http://creativecommons.org/licenses/by-nc-nd/4.0/</a>
Type	article (author version)
File Information	NUCL INSTRUM METH B426_13-17.pdf



[Instructions for use](#)

**Title**

Production cross sections of deuteron-induced reactions on natural palladium for Ag isotopes

**Authors**

Naoyuki Ukon<sup>1,2)</sup>, Masayuki Aikawa<sup>3)</sup>, Yukiko Komori<sup>4)</sup>, Hiromitsu Haba<sup>4)</sup>

**Affiliations and addresses of authors**

<sup>1</sup>Nuclear Reaction Data Center (JCPRG), Faculty of Science, Hokkaido University, Kita 10 Nishi 8, Kita-ku, Sapporo 060-0810, Japan

<sup>2</sup>Advanced Clinical Research Center, Fukushima Global Medical Science Center, Fukushima Medical University, 1 Hikariga-oka, Fukushima City 960-1295, Japan

<sup>3</sup>Faculty of Science, Hokkaido University, Kita 10 Nishi 8, Kita-ku, Sapporo 060-0810, Japan

<sup>4</sup>Nishina Center for Accelerator-Based Science, RIKEN, Wako, Saitama 351-0198, Japan

**Address correspondence to**

Naoyuki Ukon, Ph.D.

Advanced Clinical Research Center, Fukushima Global Medical Science Center,  
Fukushima Medical University, 1 Hikariga-oka, Fukushima City 960-1295, Japan

E-mail: ukon@fmu.ac.jp, Tel: +81-24-581-5169, FAX: +81-24-581-5170

**First author:**

Naoyuki Ukon, Ph.D.

Advanced Clinical Research Center, Fukushima Global Medical Science Center,  
Fukushima Medical University, 1 Hikariga-oka, Fukushima City 960-1295, Japan

E-mail: ukon@fmu.ac.jp, Tel: +81-24-581-5169, FAX: +81-24-581-5170

**Abstract**

Activation cross sections for deuteron-induced reactions on natural palladium were measured up to 24 MeV using the stacked-foil method and the high resolution gamma-ray spectroscopy. The production cross sections of  $^{103}\text{Ag}$ , the parent of a medical radioactive isotope  $^{103}\text{Pd}$ , were obtained. We found that our result is in good agreement with the previous data up to 20.3 MeV, and obtained new data at higher

energies. In addition, the production cross sections of  $^{104g+m}\text{Ag}$ ,  $^{105}\text{Ag}$ ,  $^{106m}\text{Ag}$ ,  $^{110m}\text{Ag}$  and  $^{111}\text{Ag}$  were presented.

**Key words:** Palladium, Ag isotopes, deuteron-induced reactions, cross sections, therapeutic radionuclide

**(81 words)**

## 1 Introduction

Radioisotopes (RI) are available for medical therapy and diagnostics [1].  $^{103}\text{Pd}$  with a half-life of  $T_{1/2} = 16.991$  d decays (100% electron capture (EC)) to  $^{103\text{m}}\text{Rh}$  that decays (100% isomeric transition) to  $^{103}\text{Rh}$  with the 39.5-keV  $\gamma$ -ray emission.  $^{103}\text{Pd}$  is a medical radioisotope and available for brachytherapy [2]. For the effective production of  $^{103}\text{Pd}$ , a variety of reactions should be investigated for comparison. They also include reactions to produce  $^{103}\text{Ag}$  ( $T_{1/2} = 65.7$  min), a parent of  $^{103}\text{Pd}$ . A process to produce  $^{103}\text{Ag}$  is deuteron-induced reactions on natural palladium, which has only been studied up to 20.3 MeV in the previous studies [3-5]. A radionuclide  $^{104\text{g}}\text{Ag}$  could be used as a diagnostic imaging of positron emission tomography (PET), which has the short  $\beta^+$  decay half-life ( $T_{1/2} = 69.2$  min).  $^{111}\text{Ag}$  has a potential as the therapeutic  $\beta^-$  radionuclide decaying (92%  $\beta^-$ ,  $E_{\beta\text{max}} = 1037$  keV) directly to the ground state of  $^{111}\text{Cd}$ . In addition, PET using  $^{104}\text{Ag}$  has the possible combination of diagnostic studies to investigate the uptake of  $^{111}\text{Ag}$  labelled compounds of the therapeutic radionuclide before treatment [6].  $^{103}\text{Ag}$ ,  $^{104\text{m,g}}\text{Ag}$  and  $^{111}\text{Ag}$  can be obtained by charged particle reactions on  $^{\text{nat}}\text{Pd}$ . Therefore, we investigated the activation cross sections of deuteron-induced reactions on natural palladium metal ( $^{102}\text{Pd}$  1.02%;  $^{104}\text{Pd}$  11.14%;  $^{105}\text{Pd}$  22.33%;  $^{106}\text{Pd}$  27.33%;  $^{108}\text{Pd}$  26.46%;  $^{110}\text{Pd}$  11.72%) in connection with production of medically relevant

radioisotopes.

## 2 Materials and method

### 2.1 Experimental setup

The excitation function of the deuteron-induced reactions on  $^{nat}\text{Pd}$  was measured by the stacked-foil activation method and the high resolution gamma-ray spectroscopy.  $^{nat}\text{Pd}$  target foils (thickness:  $9.80 \text{ mg/cm}^2$ , purity: 99.95%, Nilaco Corp., Japan) were stacked with  $^{nat}\text{Ti}$  foils (thickness:  $2.25 \text{ mg/cm}^2$ , purity: 99.6%, Nilaco Corp., Japan) for monitoring the beam parameters and  $^{nat}\text{Zn}$  foils (thickness:  $17.95 \text{ mg/cm}^2$ , purity: 99.95%, Nilaco Corp., Japan) for degrading the beam energy. 20, 19 and 16 foils for  $^{nat}\text{Pd}$ ,  $^{nat}\text{Ti}$  and  $^{nat}\text{Zn}$ , respectively, were selected to cover the whole energy range from the maximum energy down to the thresholds of the  $^{nat}\text{Pd}(d, x)$  reactions.

The irradiation was performed at the RIKEN AVF cyclotron. The 23.95 MeV deuteron beam with an average intensity of 174.74 nA was irradiated on the target for 20 minutes. The incident beam energy was measured by the time-of-flight method using the plastic scintillator monitor [7]. The beam energy at each target foil was calculated

using the polynomial approximation of the stopping power data [8]. The  $\gamma$ -ray spectra of the activated foils were measured by HPGe detectors (ORTEC GEM35P4-70). Nuclear decay data are taken from the online NuDat 2.7 database [9] and summarized in Table 1.

The net peak areas in the  $\gamma$ -ray spectra were analyzed by Gamma Studio (SEIKO EG&G CO.LTD.). The activation cross sections of  $^{103}\text{Ag}$ ,  $^{104\text{g+m}}\text{Ag}$ ,  $^{105\text{m}}\text{Ag}$ ,  $^{106\text{m}}\text{Ag}$ ,  $^{110\text{m}}\text{Ag}$  and  $^{111}\text{Ag}$  in the deuteron-induced reactions on  $^{\text{nat}}\text{Pd}$  were deduced by using the standard activation formula (1)

$$\sigma = \frac{T_{\gamma}\lambda}{\varepsilon_d\varepsilon_{\gamma}\varepsilon_t N_t N_b (1 - e^{-\lambda t_b}) e^{-\lambda t_c} (1 - e^{-\lambda t_m})} \quad (1)$$

where  $N_t$  denotes the surface density of target atoms,  $N_b$  the number of bombarding particles per unit time,  $T_{\gamma}$  the number of counts in photo-peak,  $\varepsilon_d$  the detector efficiency,  $\varepsilon_{\gamma}$  the gamma-ray abundance,  $\varepsilon_t$  the measurement dead time, which is the ratio of live time to real time,  $\lambda$  the decay constant,  $t_b$  the bombarding time,  $t_c$  the cooling time, and  $t_m$  acquisition time.

### 3 Results and discussion

The excitation function of the  $^{nat}\text{Ti}(d,x)^{48}\text{V}$  monitor reaction was compared with the recommended values provided by IAEA [10] to obtain the beam intensity. The cross sections of  $^{48}\text{V}$  were measured by using the 983.53 keV (99.98%) and the 1312.11 keV (98.2%)  $\gamma$ -lines from the decay of  $^{48}\text{V}$  ( $T_{1/2} = 15.9735$  d). The measurements were performed after adequate cooling time to prevent the contribution from the  $^{48}\text{Sc}$  decay ( $T_{1/2} = 43.67$  h). The excitation function of for the  $^{nat}\text{Ti}(d,x)^{48}\text{V}$  reaction is shown in Fig. 1. The measured beam intensity was normalized by the cross section to fit the recommended values of the monitor reaction, which was 6.6% higher than the measured one. The directly measured beam intensity from the Faraday cup measurement was increased by 6.6%. In the data evaluation the beam intensity deduced from monitor reaction was adopted.

The present experimental data will be discussed for each reaction product. The numerical data are summarized in Table 2. The results are compared with the previous data [3,5,6] and the TENDL-2017 online data library [11] in Figs. 2-8. The total uncertainty is estimated to be less than 21.5% including statistical uncertainty (1 – 19.64%). It was estimated as the square root of the quadratic summation of the propagating components; the beam intensity (5%), target thickness (1%), target purity (1%), and detector efficiency (5%).



### 3.1 Production of $^{103}\text{Ag}$

The excitation function of the  $^{\text{nat}}\text{Pd}(d,x)^{103}\text{Ag}$  reaction is derived from the  $\gamma$ -line at 118.7 keV (31.2%) and shown in Fig. 2 with the previous experimental data [4] and TENDL-2017 [11]. We found that our result is in good agreement with the previous data up to 20.3 MeV. We obtained new data at the higher energies.

On the other hands, the theoretical calculation agrees well with the experimental data at 15 MeV or less, but above 15 MeV, greatly overestimates. This is probably because the theoretical calculation overestimates the cross sections of the  $^{104}\text{Pd}(d,3n)^{103}\text{Ag}$  reaction.

### 3.2 Productions of $^{104\text{g}}\text{Ag}$ and $^{104\text{m}}\text{Ag}$

The radionuclide  $^{104\text{g}}\text{Ag}$  has a ground state ( $T_{1/2} = 69.2$  min) and an excited isomeric state  $^{104\text{m}}\text{Ag}$  ( $T_{1/2} = 33.5$  min). The metastable state has no independent  $\gamma$ -rays. In the previous study, based on the differences in the half-lives and the limited internal transition probability, the estimation of the total  $^{104\text{m+g}}\text{Ag}$  activity is uncertainty[6] and the experimental cross section data were found only for cumulative reaction.

On the other hand,  $^{104\text{g}}\text{Ag}$  and  $^{104\text{m}}\text{Ag}$  have different  $\gamma$ -ray abundances: 555.8

keV (92.6%) and 767.7 keV (65.7%) in  $^{104g}\text{Ag}$  and 555.8 keV (91%) and 767.7 keV (0.9%) in  $^{104m}\text{Ag}$ . Thus, we could obtain the independent cross sections of  $^{104m}\text{Ag}$  and  $^{104g}\text{Ag}$  in the measured gamma peak. The raw counts  $\Delta T^g$  and  $\Delta T^m$  of  $^{104g}\text{Ag}$  and  $^{104m}\text{Ag}$ , respectively, were calculated with the formulae (2), (3) and (4)

$$T_{\gamma_1} = \varepsilon_{d1}(\varepsilon_{\gamma_1}^g \Delta T^g + \varepsilon_{\gamma_1}^m \Delta T^m) \quad (2)$$

$$T_{\gamma_2} = \varepsilon_{d2}(\varepsilon_{\gamma_2}^g \Delta T^g + \varepsilon_{\gamma_2}^m \Delta T^m) \quad (3)$$

$$\Delta T^m = \frac{1}{\varepsilon_{d1}\varepsilon_{d2}} \frac{\varepsilon_{d2}\varepsilon_{\gamma_2}^g T_{\gamma_1} - \varepsilon_{d1}\varepsilon_{\gamma_1}^g T_{\gamma_2}}{\varepsilon_{\gamma_2}^g \varepsilon_{\gamma_1}^m - \varepsilon_{\gamma_1}^g \varepsilon_{\gamma_2}^m} \quad (4)$$

where  $T_{\gamma_1}$  and  $T_{\gamma_2}$  denote the numbers of net counts in photo-peaks  $\gamma_{m1}$  and  $\gamma_{m2}$  (555.8 and 767.7 keV),  $\varepsilon_{d1}$  and  $\varepsilon_{d2}$  the detector efficiencies in each photo-peak,  $\varepsilon_{\gamma_1}^g$ ,  $\varepsilon_{\gamma_2}^g$ ,  $\varepsilon_{\gamma_1}^m$  and  $\varepsilon_{\gamma_2}^m$  the gamma ray abundances of the ground state and the excited isomeric state in each photo-peak.

Figures 3 and 4 show the excitation functions for the  $^{nat}\text{Pd}(d,x)^{104g}\text{Ag}$  and  $^{nat}\text{Pd}(d,x)^{104m}\text{Ag}$  reactions, respectively. The experimental results are compared with the TENDL-2017. The independent cross sections for  $^{104g}\text{Ag}$  and  $^{104m}\text{Ag}$  were reported for the first time. Both cross sections show good agreement with the theoretical calculations.

### 3.3 Production of $^{105}\text{Ag}$

The  $^{105}\text{Ag}$  has a long-lived ground state  $^{105\text{g}}\text{Ag}$  ( $T_{1/2} = 41.29$  d), and an short-lived excited isomeric state  $^{105\text{m}}\text{Ag}$  ( $T_{1/2} = 7.23$  min) that decays to  $^{105\text{g}}\text{Ag}$  by an internal transition (99.66%). We could measure only the cumulative production of  $^{105\text{g}}\text{Ag}$  with its  $\gamma$ -ray of 344.52 keV (41.4%). The result of this study is in good agreement with the previous data (Fig. 5). The theoretical results of TENDL-2017 agree well with the experimental points [11].

### 3.4 Production of $^{106\text{m}}\text{Ag}$

The radionuclide  $^{106}\text{Ag}$  has a short-lived ground state ( $T_{1/2} = 23.96$  min) and an isomeric state  $^{106\text{m}}\text{Ag}$  ( $T_{1/2} = 8.28$  d). We could measure only the longer-lived isomeric state due to long cooling time. The  $\gamma$ -line at 717.34 keV (28.9%) from the decay of  $^{106\text{m}}\text{Ag}$  was used to determine the cross section for the  $^{106\text{m}}\text{Ag}$  production. The result is in good agreement with the previous data in the overlapping energy range (Fig. 6). The peak values are overestimated by TENDL-2017 [11].

### 3.5 Production of $^{110\text{m}}\text{Ag}$

The radionuclide  $^{110}\text{Ag}$  has a short-lived ground state  $^{110\text{g}}\text{Ag}$  ( $T_{1/2} = 24.5$  s) and an excited isomeric state  $^{110\text{m}}\text{Ag}$  ( $T_{1/2} = 249.8$  d) that decays to  $^{110\text{g}}\text{Ag}$  by an internal transition (1.4%) and to stable  $^{110}\text{Cd}$  by  $\beta$  decay (98.6%).  $^{110\text{m}}\text{Ag}$  emits the  $\gamma$  ray of 657.8 keV (94.6%). We could measure only the production cross sections of the long-lived isomer produced by the  $^{110}\text{Pd}(d,2n)$  reaction (Fig. 7). Our result is in good agreement with the previous ones [3, 4]. The theoretical calculation overestimates the experiment data, though the peak energy is in good agreement with the previous data. The maximum value of TENDL-2017 is 15% larger than the measured results.

### 3.6 Production of $^{111}\text{Ag}$

The radionuclide  $^{111}\text{Ag}$  has a ground state  $^{111\text{g}}\text{Ag}$  ( $T_{1/2} = 7.45$  d), and an excited isomeric state  $^{111\text{m}}\text{Ag}$  ( $T_{1/2} = 64.8$  s) that decays to  $^{111\text{g}}\text{Ag}$  by internal transition (99.3%). The ground-state of  $^{111}\text{Ag}$  is also fed from the  $\beta$ -decay (23%) of  $^{111\text{m}}\text{Pd}$ . Therefore, we could measure only the cumulative production of  $^{111\text{g}}\text{Ag}$ . The excitation function of the  $^{\text{nat}}\text{Pd}(d,x)^{111}\text{Ag}$  reaction is derived from the  $\gamma$ -line at 254.4 keV (1.33%) and shown in Fig. 8 with the previous experimental data [6] and TENDL-2017 [11].  $^{111}\text{Ag}$  is produced solely from the reactions on  $^{110}\text{Pd}$  in this experimental condition [3]. In this study, the experimental data are in acceptably good agreement with the previous data from 12 to

24 MeV. The results of TENDL-2017 [11] underestimate significantly the experimental data and an energy shift of the peak can be seen.

#### **4 Conclusions**

We performed the experiment of the deuteron-induced reactions on natural palladium to produce Ag isotopes by using the stacked foil activation technique. The excitation function of the  ${}^{\text{nat}}\text{Pd}(d,x){}^{103}\text{Ag}$  reaction from 20.3 MeV to 24 MeV,  ${}^{\text{nat}}\text{Pd}(d,x){}^{104\text{g}}\text{Ag}$  and  ${}^{\text{nat}}\text{Pd}(d,x){}^{104\text{m}}\text{Ag}$  were measured for the first time.  ${}^{105}\text{Ag}$ ,  ${}^{106\text{m}}\text{Ag}$ ,  ${}^{110\text{m}}\text{Ag}$  and  ${}^{111}\text{Ag}$  are in good agreements with the previous experimental data. All excitation functions are continued smoothly the data for these reactions above 30 MeV in previous study. [5]

#### **Declarations**

#### **List of abbreviations**

Electron capture (EC)

Positron emission tomography (PET)

### **Ethics approval and consent to participate**

Not applicable

### **Consent for publication**

Not applicable

### **Availability of data and materials**

The datasets supporting the conclusions of this article are included within the article.

### **Competing interests**

The authors declare that they have no competing interests.

### **Author's contributions**

Conception and design of the study: NU, MA

Analysis and interpretation of data: NU, MA

Collection and assembly of data: NU, MA, YK, HH

Drafting of the article: NU, MA

Critical revision of the article for important intellectual content: NU

Final approval of the article: MA, HH

### **Acknowledgements**

This work was carried out at RI Beam Factory operated by RIKEN Nishina Center and CNS, University of Tokyo, Japan. This work was partly supported by JSPS KAKENHI Grant Number 17K07004.

### **References**

- [1] J.F. Chatal, C.A. Hoefnagel, Radionuclide therapy, *Lancet* 354 (1999) 931.
- [2] A.S. Meigooni, R. Nath. A comparison of radial dose functions for  $^{103}\text{Pd}$ ,  $^{125}\text{I}$ ,  $^{145}\text{Sm}$ ,  $^{241}\text{Am}$ ,  $^{169}\text{Yb}$ ,  $^{192}\text{Ir}$ , and  $^{137}\text{Cs}$  brachytherapy sources, *Int J Radiat Oncol Biol Phys.* 22(5) (1992) 1125.
- [3] F. Ditrói, F. Tárkányi, S. Takács, A. Hermanne, A.V. Ignatyuk, M. Baba, Activation

cross-sections of deuteron induced reactions on natural palladium, Nucl. Instrum. Meth.

B 270 (2012) 61.

[4] A. Hermanne, S. Takács, F. Tárkányi, R. Bolbos, Cross section measurements of proton and deuteron induced formation of  $^{103}\text{Ag}$  in natural palladium, Radiochim. Acta 92 (2004) 215.

[5] F. Ditrói, F. Tárkányi, S. Takács, A. Hermanne, A.V. Ignatyuk, Measurement of activation cross-section of long-lived products in deuteron induced nuclear reactions on palladium in the 30–50 MeV energy range, Applied Radiation and Isotopes 128(2017)297.

[6] A. Hermanne, S. Takács, F. Tárkányi, R. Bolbos, Experimental cross sections for charged particle production of the therapeutic radionuclide  $^{111}\text{Ag}$  and its PET imaging analogue  $^{104\text{m}}\text{gAg}$ , Nucl. Instrum. Meth. B217 (2004) 193.

[7] Watanabe, T., Fujimaki, M., Fukunishi, N., Imao, H., Kamigaito, O., Kase, M., Komiyama, M., Sakamoto, N., Suda, K., Wakasugi, M., Yamada, K., 2014. Beam energy and longitudinal beam profile measurement system at RIBF. Proceedings 5th International Part. Accel. Conference (IPAC2014), 3566.

[8] SRIM: the Stopping and Range of Ions in Matter, available online <  
<http://www.srim.org>>.



- [9] NuDat 2.7, 2011. National Nuclear Data Center database, Data available online [⟨http://www.nndc.bnl.gov/nudat2/⟩](http://www.nndc.bnl.gov/nudat2/).
- [10] Tárkányi, F., Takács, S., Gul, K., Hermanne, A., Mustafa, M.G., Nortier, M., Oblozinsky, P., Qaim, S.M., Scholten, B., Shubin, Y.N., Youxiang, Z., 2007. Charged particle crosssection database for medical radioisotope production: diagnostic radioisotopes and monitor reactions, IAEA-TECDOC 1211. Updated web-version at [⟨http://www-nds.iaea.org/medical/⟩](http://www-nds.iaea.org/medical/).
- [11] TENDL-2017: TALYS-based evaluated nuclear data library, Data available online [⟨https://tendl.web.psi.ch/tendl\\_2017/tendl2017.html⟩](https://tendl.web.psi.ch/tendl_2017/tendl2017.html).

**Table 1**

Table 1: The investigated reactions and decay data of reaction products

Reaction product	$T_{1/2}$	Decay mode (%)	$E_\gamma$ (keV)	$I_\gamma$ (%)	Contributing reactions	Q-value (MeV)	Ref.
$^{103}\text{Ag}$	65.7 min	$\varepsilon+\beta^+$ (100)	118.7	31.2	$^{102}\text{Pd}(d, n)$	1.9	[3]
			148.2	28.3	$^{104}\text{Pd}(d, 3n)$	-15.7	
			266.9	13.3			
			531.9	8.8			
			1273.8	9.4			
$^{104g}\text{Ag}$	69.2 min	$\varepsilon+\beta^+$ (100)	555.8	92.6	$^{104}\text{Pd}(d, 2n)$	-7.3	[6]
			767.7	65.7	$^{105}\text{Pd}(d, 3n)$	-14.4	
			857.9	10.4			
			941.6	25			
			1341.8	7.3			
$^{104m}\text{Ag}$	33.5 min	$\varepsilon+\beta^+$ (99.93) IT (<0.07)	555.8	90	Same as for $^{104g}\text{Ag}$		
			767.7	0.9			
			1341.8	1.6			
$^{105}\text{Ag}$	41.29 d	$\varepsilon+\beta^+$ (100)	280.44	30.2	$^{104}\text{Pd}(d, n)$	2.742	[3]
			344.52	41.4	$^{105}\text{Pd}(d, 2n)$	-4.351	
			443.37	10.5	$^{106}\text{Pd}(d, 3n)$	-13.912	
			644.55	11.1			

$^{106m}\text{Ag}$	8.82 d	$\varepsilon$ (100)	221.701	6.6	$^{105}\text{Pd}(d, n)$	3.588	[3]
			406.182	13.4	$^{106}\text{Pd}(d, 2n)$	-5.972	
			429.646	13.2	$^{108}\text{Pd}(d, 4n)$	-21.736	
			450.976	28.2			
			616.17	21.6			
			717.34	28.9			
			748.36	20.6			
			824.69	15.3			
			1045.83	29.6			
			1128.02	11.8			
			1199.39	11.2			
			1527.65	16.3			
			$^{110m}\text{Ag}$	249.8 d	$\beta^-$ (98.6) IT (1.4)	657.8	95.6
763.9	22.6						
884.7	75.0						
937.5	35.0						
$^{111}\text{Ag}$	7.45 d	$\beta^-$ (100)	245.4	1.24	$^{110}\text{Pd}(d, n)$	2.742	[6]
			342.1	6.7	$^{110}\text{Pd}(d, p)^{111}\text{Pd}(\beta^-)$	3.501	

**Table 2**

Table 2: Measurement cross sections of the Ag isotopes

Energy (MeV)	$^{103}\text{Ag}$ (mb)	$^{104g}\text{Ag}$ (mb)	$^{104m}\text{Ag}$ (mb)	$^{105}\text{Ag}$ (mb)	$^{106m}\text{Ag}$ (mb)	$^{110m}\text{Ag}$ (mb)	$^{111}\text{Ag}$ (mb)
$23.8 \pm 0.1$	$47.3 \pm 4.9$	$132.6 \pm 10.4$	$12.4 \pm 6.6$	$300.9 \pm 23.6$	$34.6 \pm 2.9$	$12.2 \pm 1.4$	$13.0 \pm 2.4$
$23.6 \pm 0.1$	$45.3 \pm 4.7$	$131.7 \pm 10.3$	$30.7 \pm 6.0$	$297.6 \pm 23.4$	$34.6 \pm 2.9$	$12.9 \pm 1.4$	$9.9 \pm 2.3$
$22.2 \pm 0.1$	$40.7 \pm 4.2$	$145.6 \pm 11.4$	$30.5 \pm 5.3$	$338.0 \pm 26.5$	$51.6 \pm 4.3$	$14.1 \pm 1.6$	$14.7 \pm 2.8$
$22.0 \pm 0.1$	$34.5 \pm 3.6$	$125.8 \pm 9.9$	$30.1 \pm 4.4$	$292.5 \pm 23.0$	$46.9 \pm 3.9$	$13.0 \pm 1.5$	$15.0 \pm 2.5$
$20.0 \pm 0.1$	$22.9 \pm 2.4$	$142.2 \pm 11.1$	$34.8 \pm 4.2$	$344.4 \pm 27.1$	$81.5 \pm 6.8$	$19.2 \pm 2.1$	$18.9 \pm 3.4$
$19.7 \pm 0.1$	$20.7 \pm 2.2$	$142.7 \pm 11.2$	$39.4 \pm 4.0$	$351.2 \pm 27.6$	$87.3 \pm 7.2$	$19.8 \pm 2.1$	$16.2 \pm 3.2$
$17.6 \pm 0.1$	$3.3 \pm 0.4$	$109.0 \pm 8.5$	$35.1 \pm 3.3$	$336.3 \pm 26.4$	$116.2 \pm 9.6$	$27.7 \pm 2.8$	$19.6 \pm 3.8$
$17.3 \pm 0.1$	$2.1 \pm 0.3$	$95.7 \pm 7.5$	$36.1 \pm 3.2$	$325.6 \pm 25.6$	$117.9 \pm 9.8$	$28.4 \pm 2.8$	$23.2 \pm 3.9$
$14.9 \pm 0.1$	$1.5 \pm 0.3$	$76.5 \pm 6.0$	$30.8 \pm 2.6$	$293.0 \pm 23.0$	$114.8 \pm 9.5$	$40.8 \pm 3.8$	$29.2 \pm 4.3$

$12.2 \pm 0.2$	$2.0 \pm 0.3$	$53.7 \pm 4.2$	$28.0 \pm 2.3$	$251.2 \pm 19.7$	$76.8 \pm 6.4$	$36.7 \pm 3.4$	$33.9 \pm 4.4$
$9.0 \pm 0.2$	$3.6 \pm 0.4$	$12.9 \pm 1.0$	$8.6 \pm 0.7$	$186.0 \pm 14.6$	$29.8 \pm 2.5$	$16.6 \pm 1.5$	$45.7 \pm 5.0$
$5.8 \pm 0.3$	$0.6 \pm 0.1$	$0.1 \pm 0.04$	$0.04 \pm 0.02$	$20.2 \pm 1.6$	$3.2 \pm 0.3$	$0.7 \pm 0.1$	$18.0 \pm 1.9$

Figure 1

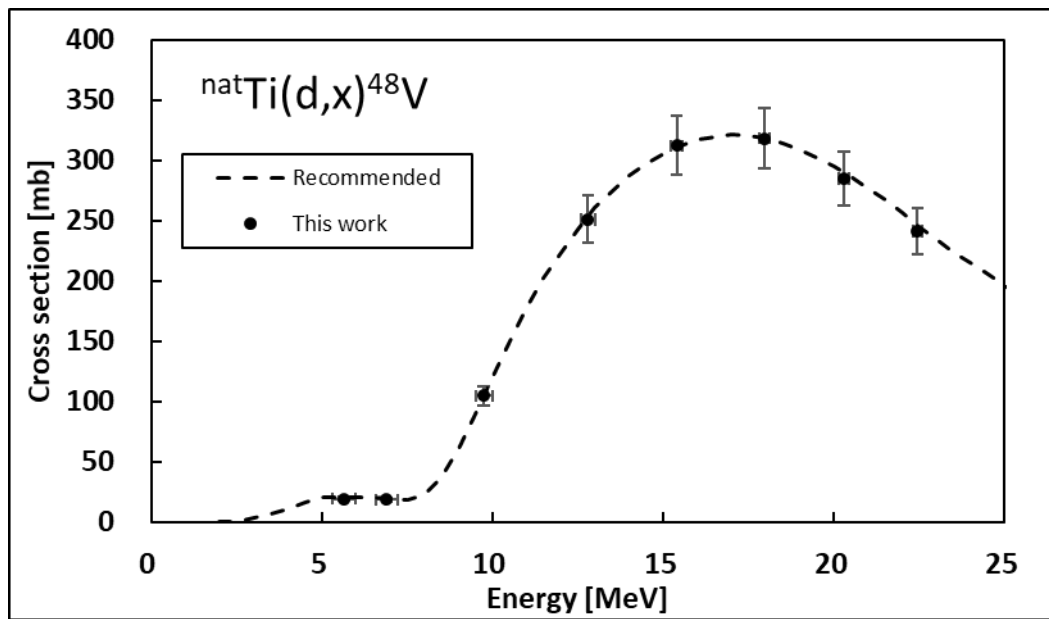


Fig. 1: The excitation function of the monitor reaction  ${}^{\text{nat}}\text{Ti}(d,x){}^{48}\text{V}$

Figure 2

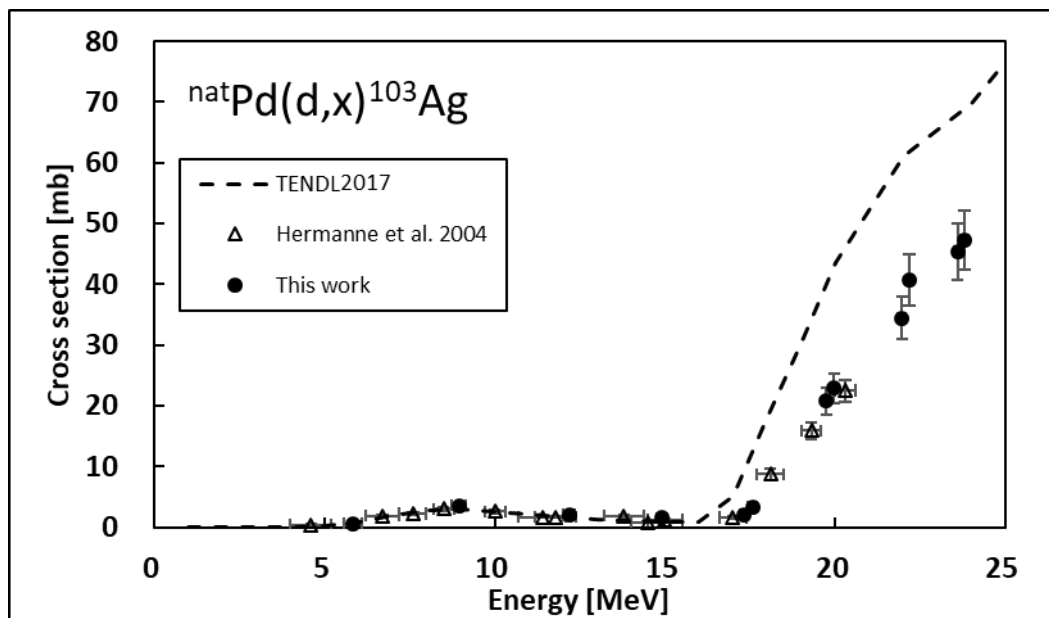


Fig. 2: The excitation function of the  ${}^{\text{nat}}\text{Pd}(d,x){}^{103}\text{Ag}$  reaction

Figure 3

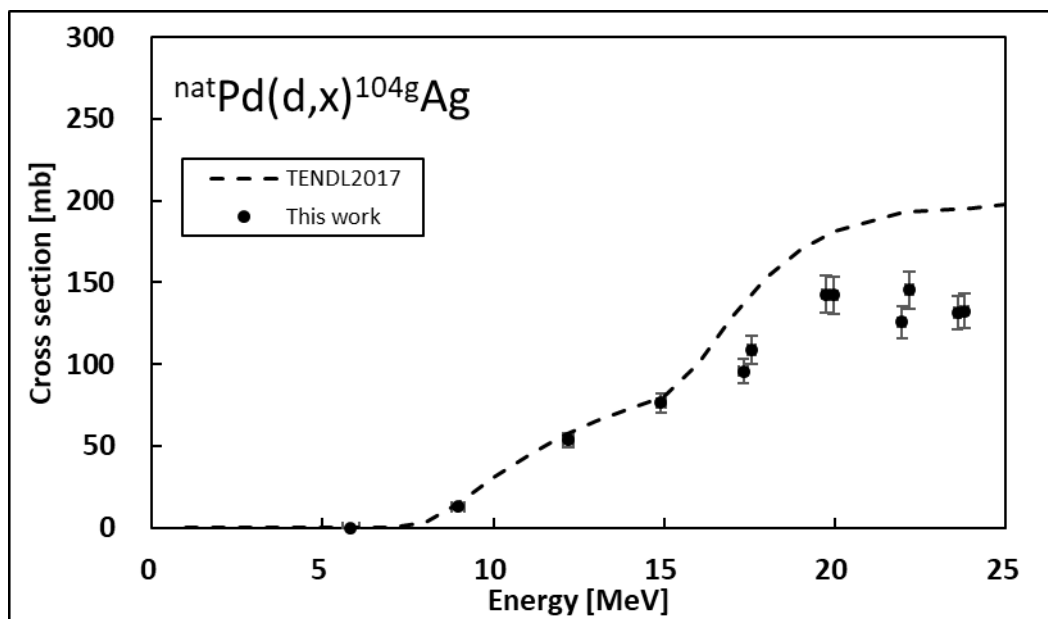


Fig. 3: The excitation function of the  ${}^{\text{nat}}\text{Pd}(\text{d},\text{x}){}^{104\text{g}}\text{Ag}$  reaction

Figure 4

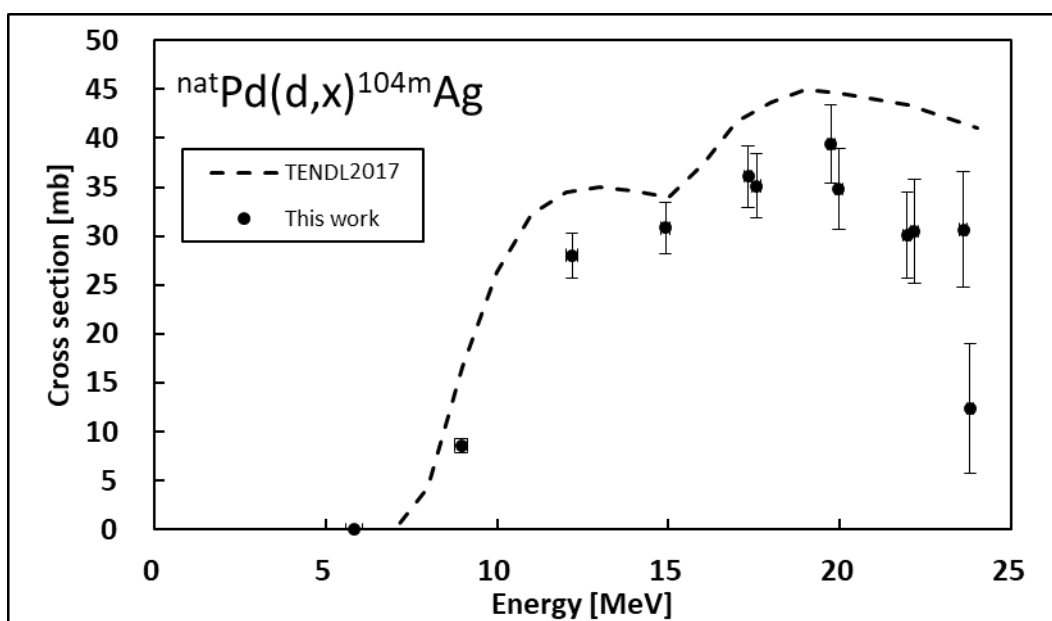


Fig. 4: The excitation function of the  $^{nat}\text{Pd}(d,x)^{104m}\text{Ag}$  reaction

Figure 5

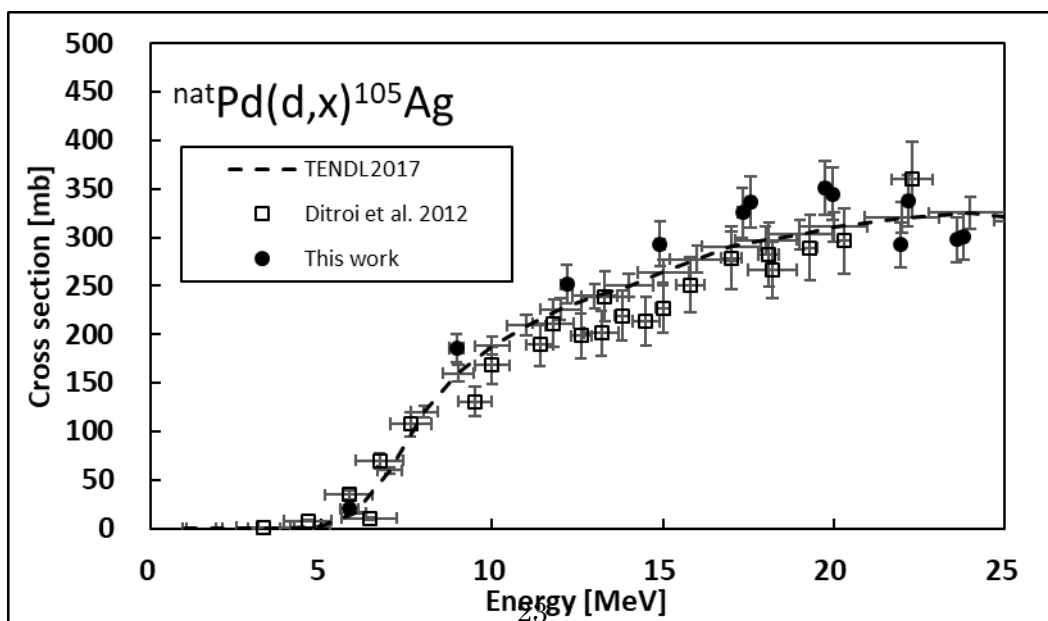




Fig. 5: The excitation function of the  $^{nat}\text{Pd}(d,x)^{105}\text{Ag}$  reaction

Figure 6

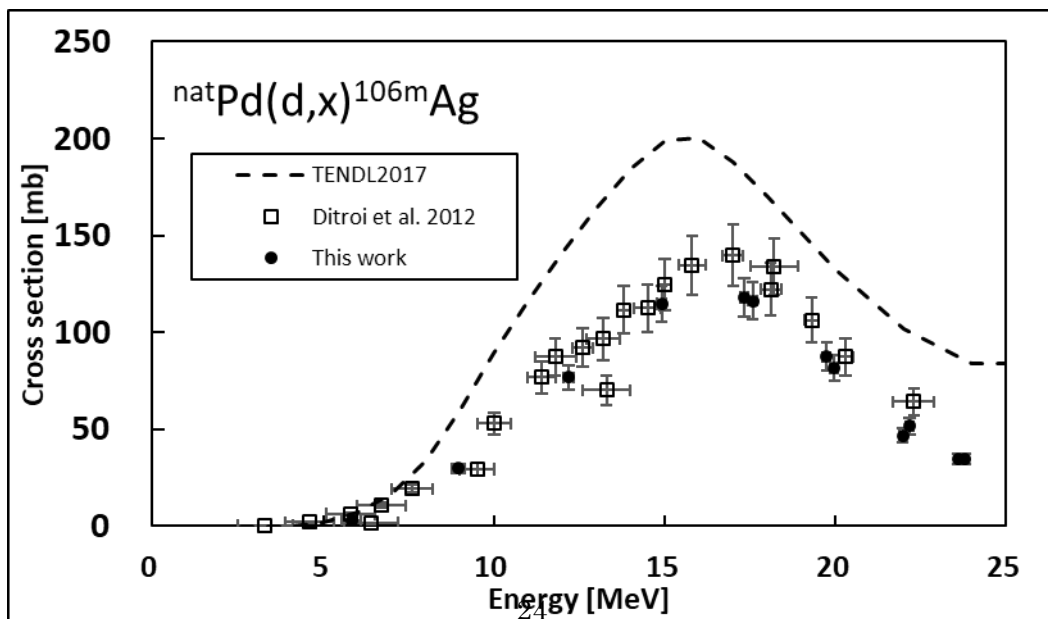


Fig. 6: The excitation function of the  $^{\text{nat}}\text{Pd}(d,x)^{106\text{m}}\text{Ag}$  reaction

Figure 7

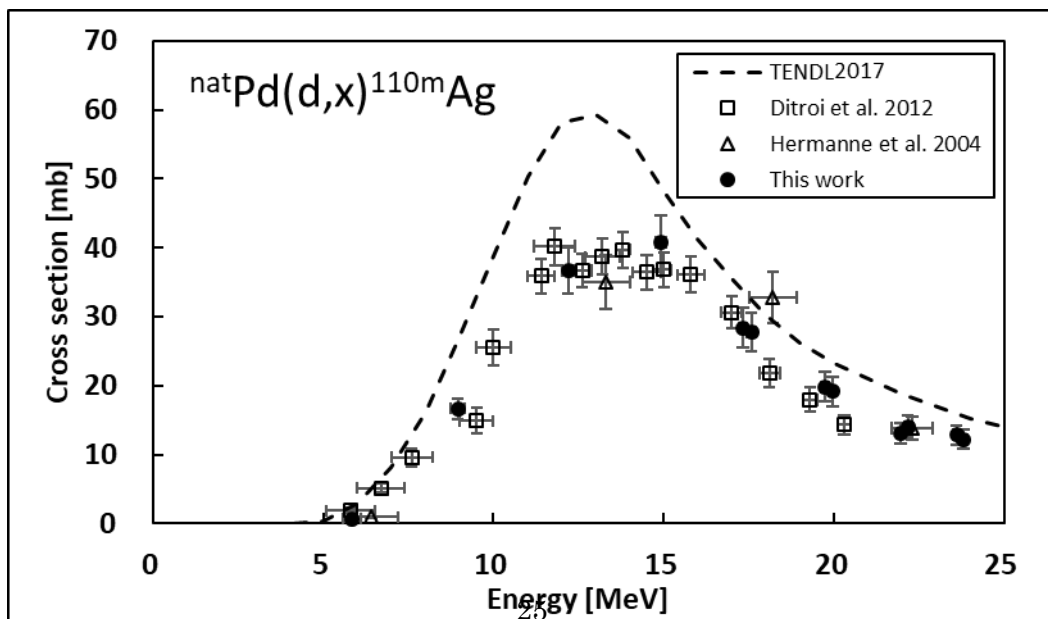


Fig. 7: The excitation function of the  $^{nat}\text{Pd}(d,x)^{110m}\text{Ag}$  reaction

Figure 8

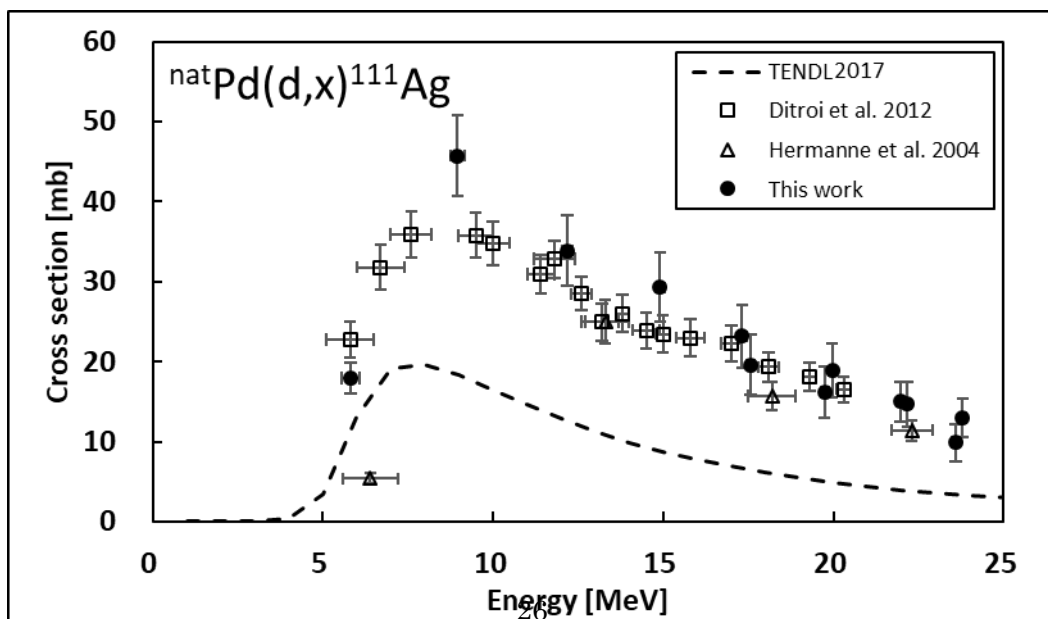


Fig. 8: The excitation function of the  $^{nat}\text{Pd}(d,x)^{111}\text{Ag}$  reaction